Eur. Phys. J. C (2018) 78:42
https://doi.org/10.1140/epjc/s10052-017-5478-1

THE EUROPEAN PHYSICAL JOURNAL C

CrossMark

Regular Article - Theoretical Physics

Direct searches of Type-III seesaw triplet fermions at high energy e^+e^- collider

Deepanjali Goswami[a], **P. Poulose**[b]

Department of Physics, Indian Institute of Technology Guwahati, Guwahati, Assam 781039, India

Received: 7 August 2017 / Accepted: 19 December 2017 / Published online: 18 January 2018
© The Author(s) 2018. This article is an open access publication

Abstract The signatures of heavy fermionic isotriplets (Σ) are probed through their direct production and subsequent decay at high energy electron–positron colliders. Unlike the case of LHC, the production process has strong dependence on the mixing of Σ with electron (V_e), making the leptonic collider unique to fingerprint the presence of such mixing. We establish that pair production considered at $\sqrt{s} = 2$ TeV can be employed to study both the cases of $V_e = 0$ and of $V_e \neq 0$ with ~ 100 fb^{-1} luminosity, while the single production can probe the latter case with a few inverse femto barn luminosity at $\sqrt{s} = 1$ TeV. Exploring the mass reach, both the single and pair productions are capable of probing Σ of mass close to the kinematic limits through selected channels. Investigating simultaneous limits on the $M_\Sigma - V_e$ parameter space, we identify suitable final states and their 3σ reach on V_e and M_Σ at 300 (100) fb^{-1} luminosity in the case of pair (single) Σ production.

1 Introduction

The Standard Model (SM) of particle physics has established itself firmly as the description of the dynamics of elementary particles at the electroweak scale. All measurements at the LHC conform to this, including the information on the Electroweak Symmetry Breaking (EWSB). However, many features, including the lack of a mechanism to generate masses for neutrinos, absence of a candidate for dark matter, inability to explain the baryon asymmetry of the universe, along with other technical issues like the mechanism to stabilise the Higgs boson mass against quantum corrections, force us to look beyond the SM. It is expected that new physics should show up in the TeV range of energies. Concerning the mechanism to generate mass to the neutrinos, the seesaw mechanism [1–7] has emerged as the most popular and perhaps the most viable way of generating a tiny mass of the observed light neutrinos of three different flavours. The seesaw mechanism effectively exploits this idea by introducing lepton number violating Majorana mass terms, either directly or generated dynamically. The tininess of the neutrino mass [8] in this case is achieved with the help of a large mass scale present in the scenario, usually brought about as the mass of a heavy partner. Generically, the seesaw mechanism is categorised into three types. In the Type-I seesaw model [1–6], a minimum of two gauge singlet right-handed neutrino fields are introduced in addition to the SM fields. In this case, the light neutrino mass is inversely proportional to the mass of this new partner fermion, thus allowing it to be naturally small in the presence of a heavy partner. In the Type-II seesaw model [9–15] $SU(2)_L$ triplet scalar fields with hypercharge $Y = 2$ are introduced. The vacuum expectation value (vev) acquired by these triplet scalars induces a Majorana mass to the neutrinos. In the Type-III seesaw model [16] fermionic triplet fields with $Y = 0$ are introduced, having a Yukawa term involving the SM lepton doublet and the SM Higgs field, and with Majorana mass terms. This third scenario leaves both charged as well as neutral heavy fermions in the spectrum. It is possible that such additional fermions have masses in the range of TeV, and thus could possibly be searched for at the LHC and at the proposed high energy leptonic colliders like the International Linear Collider (ILC) [17–26] or the Compact Linear Collider (CLIC) [27–30]. Generically, we shall refer to these high energy leptonic collider facilities as the Future Leptonic Colliders (FLCs). The phenomenology of the Type-III seesaw model in the context of LHC has been carried out in some detail by many authors [31–38]. Experimental searches for the additional charged, as well as neutral heavy fermions arising in this model are performed by both CMS and ATLAS. Considering data from the $\sqrt{s} = 13$ TeV run, CMS [39] has set a lower limit of 430 GeV on the triplet mass. The ATLAS results [40,41] rule out masses in the range

[a] e-mail: g.deepanjali@iitg.ernet.in

[b] e-mail: poulose@iitg.ernet.in

below 325–540 GeV under the specific scenarios considered. The larger value corresponds to the assumption of decay of the heavy neutral fermion exclusively to $W\ell$, and the heavy charged fermion to $W\nu$. The Yukawa interaction term leading to the off-diagonal mass matrix for the neutral fermions also causes mixing in the charged lepton sector. Simultaneous presence of the mixing with two flavours receive very stringent constraints from Lepton Flavour Violating (LFV) decays like $\mu \to e\gamma$, eee, and $\tau \to \mu\gamma$, $e\gamma$. However, if the mixing is restricted to a single flavour, it could be large enough (constrained by the electroweak precision data) to leave its effects at the colliders. The latter case is, however, not possible to probe at the LHC, when one restricts oneself to pair production of the heavy fermions, as the mixing parameter cancels out in the branching fraction. The cross section for single production of heavy fermion in association with SM leptons has the potential to probe the mixing at the production level. However, this cross section is too small to investigate at the LHC. For example, $pp \to \Sigma^+ e^-$ has a cross section of 0.047 fb with a maximally allowed mixing of $V_e = 0.05$ and the most optimistic scenario of $M_\Sigma = 500$ GeV. On the other hand, at the leptonic colliders, the production itself is sensitive to the mixing, as we shall describe in detail later. Single production of the charged and neutral heavy fermions in the electron–proton collider (LHeC) is studied in Ref. [42]. While there are studies of the indirect influence of the presence of triplet fermions in the context of Higgs pair production at the ILC [43], the direct production is not explored to the best of our knowledge. The advantages of the leptonic colliders, being sensitive to the mixing at the production level, as well as their clean environment, are exploited in the present study in which we shall investigate the possible reach of the high energy e^-e^+ collider in searching for heavy fermions, and we discuss the sensitivity to the mixing. Here we envisage a scenario with sufficiently large mixing between the heavy leptons and the SM leptons. However, the compatibility of a large mixing scenario will be in conflict with generating small neutrino mass in pure Type-III seesaw models. We shall anticipate extended versions of the seesaw mechanism, like for example the inverse seesaw mechanism to invoke a small neutrino mass, at the same time allowing for large Yukawa couplings, and consequently large mixing. In such extended scenarios, the low energy (TeV scale) spectrum is assumed to be that of the simple Type-III seesaw mechanism, with all other particles beyond the kinematic reach of the colliders being considered here. From this point of view, although the study is made in the context of the Type-III seesaw model, the conclusions can be easily adapted to any model in which such triplet fermions are present with sufficiently large mixing with the SM leptons.

We focus our attention on the production of both charged and neutral fermion triplets at the FLC and explore the identification of these triplets over the SM backgrounds in different channels. In particular, we shall discuss how the mixing can be probed through the processes studied here. We may note that, in a realistic seesaw model, we need at least two triplet fields in order to accommodate the observed mass splittings of the three neutrino flavours. However, in this study, for simplicity, we shall consider a single family of triplet fermion fields in addition to the SM fields. In a more realistic case, this may be considered equivalent to the case when the other fermions are much heavier, and therefore it would not be relevant to the phenomenology at the energies considered.

We organise this article as follows. In Sect. 2 we shall discuss some details of the Type-III seesaw model. In Sect. 3 we shall describe the processes under study, and discuss the results. Finally, we shall summarise and conclude in Sect. 5.

2 Type-III seesaw model

In this section we shall describe the features of the Type-III seesaw model relevant to our discussion. We have used the FeynRules implementation of the model as explained in Ref. [44]. Therefore, for convenience, we shall follow the notations and conventions used in this reference. The Lagrangian involving the $SU(2)_L$ triplet fermion field, denoted here as Σ, along with the SM part denoted by $\mathcal{L}_{SM}$, is given by $\mathcal{L} = \mathcal{L}_{SM} + \mathcal{L}_\Sigma$, with

$$\mathcal{L}_\Sigma = \mathrm{Tr}\big(\bar{\Sigma}\, i\not{D}\Sigma\big) - \frac{1}{2} M_\Sigma\, \mathrm{Tr}\left(\bar{\Sigma}\Sigma^c + \bar{\Sigma}^c\Sigma\right) - \sqrt{2}\, Y_{\Sigma l}\, \left(\tilde{\phi}^\dagger \bar{\Sigma} L - \bar{L}\Sigma\tilde{\phi}\right), \tag{1}$$

where M_Σ is the mass parameter of the triplet and $Y_{\Sigma l}$ is for the Yukawa couplings corresponding to the lepton flavours $l = e,\ \mu,\ \tau$. The left-handed lepton doublets of the SM are denoted by $L \equiv (\nu, l)^T$, and the Higgs doublet by $\phi \equiv (\phi^+,\ \phi^0)^T \equiv (\phi^+,\ (v + H + i\eta)/\sqrt{2})^T$, with $\tilde{\phi} = i\tau_2\, \phi^*$. The fermion triplet Σ is explicitly given by

$$\Sigma = \begin{pmatrix} \Sigma^0/\sqrt{2} & \Sigma^+ \\ \Sigma^- & -\Sigma^0/\sqrt{2} \end{pmatrix} \tag{2}$$

and its conjugate is denoted by $\Sigma^c \equiv C\bar{\Sigma}^T$, where C is the charge conjugation operator.

The two-component charged spinors are combined into the Dirac spinor $\Psi \equiv \Sigma_R^{+c} + \Sigma_R^-$, with $\Psi_R \equiv \Sigma_R^-$, and $\Psi_L \equiv \Sigma_R^{+c}$, to conveniently express the mixing of the SM charged leptons with the triplets, whereas the neutral component, Σ^0, is left as the two-component Majorana fermion. The Lagrangian in the new set-up is given by

$$\mathcal{L}_\Sigma = \overline{\Psi} i\not{\partial}\Psi + \overline{\Sigma}_R^0 i\not{\partial}\Sigma_R^0 - g\, W_\mu^3\, \bar{\Psi}\gamma^\mu\Psi + g\left(W_\mu^+\, \bar{\Sigma}_R^0\gamma^\mu P_R\Psi + W_\mu^+\, \bar{\Sigma}_R^{0c}\gamma^\mu P_L\Psi + h.c.\right)$$

$$- M_\Sigma \bar{\Psi}\Psi - \left(\frac{1}{2} M_\Sigma \ \bar{\Sigma}_R^0 \Sigma_R^{0c} + h.c\right) - \sum_\ell Y_{\Sigma\ell} \left(\phi^0 \bar{\Sigma}_R^0 \nu_L + \sqrt{2}\phi^0 \bar{\Psi} \ell_L + \phi^+ \bar{\Sigma}_R^0 \ell_L - \sqrt{2}\phi^+ \bar{\nu}_{\ell L}^c \Psi + h.c.\right). \quad (3)$$

An expanded form of the Lagrangian in the mass basis is presented in Appendix A1, which provides various couplings explicitly. Mixing between the heavy fermion, Σ and the SM leptons ($\ell = e,\ \mu,\ \tau$) are denoted by $V_\ell = \frac{v}{\sqrt{2}M_\Sigma} Y_{\Sigma\ell}$. The search for flavour changing rare decays, $\mu \to e\gamma$, $\tau \to \mu\gamma$ and $\tau \to e\gamma$, imposes stringent constraints on the couplings with the latest limits given by [44–47]

$$|V_e V_\mu| < 1.7 \times 10^{-7},\ \ |V_e V_\tau| < 4.2 \times 10^{-4},\ \ |V_\mu V_\tau| < 4.9 \times 10^{-4}. \quad (4)$$

However, these constraints will not be applicable if only one type of mixing is assumed to be present. In that case, the single parameter bounds obtained from electroweak precision measurements are much weaker, with the latest limits given by [47]

$$|V_e| < 0.055,\ \ |V_\mu| < 0.063,\ \ |V_\tau| < 0.63. \quad (5)$$

The presence of mixing allows the triplet fermions to decay to the SM final states involving leptons, gauge bosons and the Higgs boson, through the off-diagonal charged-current and neutral current interactions. The decay widths of different channels depend on the masses and mixings as given by [32]

$$\Gamma\left(\Sigma^0 \to \ell^\pm W^\mp\right) = \frac{g^2}{64\pi}|V_\ell|^2 \frac{M_\Sigma^3}{M_W^2} \times \left(1 - \frac{M_W^2}{M_\Sigma^2}\right)^2 \left(1 + 2\frac{M_W^2}{M_\Sigma^2}\right),$$

$$\Gamma\left(\Sigma^0 \to \sum_\ell \nu_\ell Z\right) = \frac{g^2}{64\pi \cos^2\theta_W} \sum_\ell |V_\ell|^2 \frac{M_\Sigma^3}{M_Z^2} \times \left(1 - \frac{M_Z^2}{M_\Sigma^2}\right)^2 \left(1 + 2\frac{M_Z^2}{M_\Sigma^2}\right),$$

$$\Gamma\left(\Sigma^0 \to \sum_\ell \nu_\ell H\right) = \frac{g^2}{64\pi} \sum_\ell |V_\ell|^2 \frac{M_\Sigma^3}{M_W^2} \left(1 - \frac{M_H^2}{M_\Sigma^2}\right)^2,$$

$$\Gamma\left(\Sigma^\pm \to \sum_\ell \nu_\ell W^\pm\right) = \frac{g^2}{32\pi} \sum_\ell |V_\ell|^2 \frac{M_\Sigma^3}{M_W^2} \times \left(1 - \frac{M_W^2}{M_\Sigma^2}\right)^2 \left(1 + 2\frac{M_W^2}{M_\Sigma^2}\right),$$

Table 1 Branching ratio of the charged and neutral triplet fermion with mass, $M_\Sigma = 500$ GeV, with only one of V_ℓ considered to be present, setting the other two to zero

Decay $\Sigma^\pm$	Decay Σ^0	BR in %
$\Sigma^\pm \to W^\pm \nu$	$\Sigma^0 \to W\ell$	51
$\Sigma^\pm \to Z\ell^\pm$	$\Sigma^0 \to Z\nu$	26
$\Sigma^\pm \to H\ell^\pm$	$\Sigma^0 \to H\nu$	23

$$\Gamma\left(\Sigma^\pm \to \ell^\pm Z\right) = \frac{g^2}{64\pi \cos^2\theta_W}|V_\ell|^2 \frac{M_\Sigma^3}{M_Z^2} \times \left(1 - \frac{M_Z^2}{M_\Sigma^2}\right)^2 \left(1 + 2\frac{M_Z^2}{M_\Sigma^2}\right)$$

$$\Gamma\left(\Sigma^\pm \to \ell^\pm H\right) = \frac{g^2}{64\pi}|V_\ell|^2 \frac{M_\Sigma^3}{M_W^2} \left(1 - \frac{M_H^2}{M_\Sigma^2}\right)^2. \quad (6)$$

Here g is the $SU(2)_L$ gauge coupling, θ_W is the Weinberg mixing angle, and M_W, M_Z and M_H are the masses of the gauge bosons and the Higgs boson, respectively. The individual decay widths, and thus the total width, has the usual strong dependence on the mass of the decaying Σ. However, this strong dependence cancels in the branching ratio (BR), leaving it practically independent of the mass for heavy fermions of mass beyond 500 GeV. This is especially facilitated by the fact that the masses of the gauge bosons and the Higgs boson are all approximately around 100 GeV. From Eq. (6) it may also be noted that when only one mixing is present we have $\Gamma(\Sigma^0 \to \sum_\ell \ell^\pm W^\mp) = \Gamma(\Sigma^\pm \to \sum_\ell \nu_\ell W^\pm)$, $\Gamma(\Sigma^0 \to \sum_\ell \nu_\ell Z) = \Gamma(\Sigma^\pm \to \ell^\pm Z)$ and $\Gamma(\Sigma^0 \to \sum_\ell \nu_\ell H) = \Gamma(\Sigma^\pm \to \sum_\ell \nu_\ell W^\pm)$, thus resulting in the same BRs to the respective channels in both the cases, as presented in Table 1 for $M_\Sigma = 500$ GeV. This is naturally expected, as all the decays are facilitated by the same Yukawa interaction term inducing mixing between the heavy fermions and the SM leptons, and the topology of the two body decays keeps the phase space factor the same. Of the charged (neutral) triplets, about 51% decay to $W\nu$ ($W\ell$), and 26% to $Z\ell$ ($Z\nu$), with 23% decaying to $H\ell$ ($H\nu$). For the reasons mentioned above, these fractions remain the same for masses above 500 GeV, assuming only one of the V_ℓ is non-zero.

Direct production of Σ at the LHC goes through the single production process, $pp \to \ell\Sigma^{0,\pm}$, $\nu\Sigma^{0,\pm}$ with s-channel quark annihilation mediated by Z or W, and the pair production, $pp \to \Sigma^{0,+}\Sigma^{0,-}$ mediated by the Z or γ. The production cross sections for the best case scenario of $M_\Sigma = 500$ GeV and $V_e = 0.05$[1] is presented in Table 2 (right). While

[1] Strictly within the framework of Type-III seesaw, for $M_\Sigma \sim 1$ TeV lead to a Yukawa coupling of $\sim 10^{-6}$. This corresponds to a mixing of the same order of the Yukawa in this model. However, we envisage

Table 2 Cross sections for different production processes at 14 TeV LHC and 2 TeV e^+e^- colliders. In the case of LHC, $\ell = e,\ \mu$ corresponding to the two combinations of ($V_e = 0.05,\ V_\mu = 0$) or ($V_\mu = 0.05,\ V_e = 0$), respectively. The two above mixing scenarios give identical results in the case of LHC processes with ν in the final state, whereas the pair production processes are independent of the mixing. The mixing in the case of e^+e^- collider is as explicitly mentioned. The mass of the fermion is taken to be $M_\Sigma = 500$ GeV

Process	Cross section (fb)
$pp \to \Sigma^+\Sigma^-$	17.9
$pp \to \Sigma^0\Sigma^0$	4.57×10^{-6}
$pp \to \Sigma^\mp\ell^\pm$	0.1143
$pp \to \Sigma^0\ell^\pm$	0.1092
$pp \to \Sigma^0\nu$	0.062
$pp \to \Sigma^\pm\nu$	0.2329

Process	Cross section (fb)		
	$V_e = 0.05$ $V_\mu = 0$	$V_e = 0$ $V_\mu = 0.05$	$V_e = 0$ $V_\mu = 0$
$e^+e^- \to \Sigma^+\Sigma^-$	42.8	55.67	55.81
$e^+e^- \to \Sigma^0\Sigma^0$	0.48	2.47×10^{-5}	0
$e^+e^- \to \Sigma^\mp e^\pm$	19.13	0	0
$e^+e^- \to \Sigma^\mp\mu^\pm$	0	0.054	0
$e^+e^- \to \Sigma^0\nu$	246.2	0.027	0

considering the present best case scenario, we are aware of the LHC future run projections, where possibly regions up to $M_\Sigma \sim 1$ TeV can be explored with moderate luminosity of 300 fb^{-1}, which can go even up to 1.5 TeV with its high luminosity option [38]. However, these conclusions are sensitive to the inherent uncertainties and assumptions that require in the case of a hadronic machine like the LHC. In this study, we shall go further to find the reach of high energy electron–positron colliders on the mass, and find that it is mostly limited by the kinematics, and thus its reach can get close to $M_\Sigma = \sqrt{s}$ in the case of single production, and $M_\Sigma = \frac{\sqrt{s}}{2}$ in the case of pair production. A similar reach on the mixing parameter is also obtained. The pair production mechanism being independent of the mixing, it is hard to obtain information regarding the mixing parameters at LHC. Firstly, the pair production mechanisms involve gauge couplings of the triplets, and therefore the dependence on mixing is not significant. The decay widths, on the other hand, have a strong dependence on the mixings. However, in the total cross section, which is a product of the production cross section and branching ratio of the decay channel considered, this dependence is cancelled, as long as the heavy flavour mixes with one flavour of the SM leptons. The single production processes have a too small cross section to be of significance even in the best case scenario.

The e^+e^- colliders on the other hand have the advantage that the production mechanism itself could depend on the electron–triplet mixing parametrised by V_e, directly through the couplings of the form $e\Sigma V$, where $V = W, Z$, in the case of both pair production as well as the single production of the heavy fermions. To illustrate this the cross sections of different processes are given in Table 2 (right), for the case of $M_\Sigma = 500$ GeV and different combinations of V_ℓ. Details including the relevant Feynman diagrams are given in the next section.

3 Direct production of the triplets

In this section we shall consider the details of the single as well as pair production of both the neutral and charged triplet fermions at the high energy e^+e^- colliders.

3.1 Single production of Σ^0 and $\Sigma^\pm$

The single productions of neutral and charged components of the fermion triplet along with a neutrino or lepton, respectively, are sensitive to the mixing of these heavy fermions with the SM leptons at the production level. The Feynman diagrams involve an s-channel exchange of gauge bosons. In addition, when $V_e \neq 0$ the process receives a t-channel contribution, as shown in Fig. 1. The Higgs mediated diagram is not included as the contributions from this are negligible in the high energy lepton colliders, where the electrons can be considered to be practically massless.

The expressions for cross sections of different cases are given in Appendix A2. From the Feynman diagrams, it is clear that the cross section is proportional to $\sum_\ell |V_\ell|^2$ in the case of neutral triplet production, and to the individual $|V_\ell|^2$ in the case of charged triplet production. It is expected that the s-channel contribution falls off with increasing $\sqrt{s}$, and thus become negligible at high energies considered here. On the other hand, the t-channel contribution and the interference between the t- and the s-channel give substantial contribu-

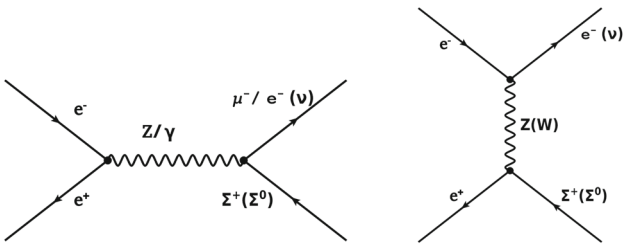

Fig. 1 Feynman diagrams contributing to the process $e^+e^- \to \Sigma^+\ell^-$ ($\Sigma^0\nu$). Note that $\Sigma^0\nu$ production does not have a photon mediated s-channel contribution

Footnote 1 continued
an extended scenario with additional mechanisms to generate a small neutrino mass, at the same time allowing large Yukawa coupling.

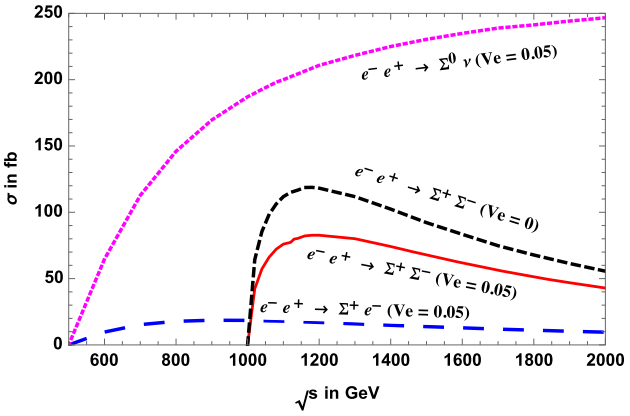

Fig. 2 Cross section for $e^+e^- \to \Sigma^0\nu$, $\Sigma^\pm e^\mp$, $\Sigma^+\Sigma^-$ against the centre-of-mass energy, with $M_\Sigma = 500$ GeV

tions when $V_e \neq 0$. We consider two different cases of (i) $V_e \neq 0$, $V_\mu = 0$, and (ii) $V_e = 0$, $V_\mu \neq 0$, with $V_\tau = 0$ in both cases. The first case leads to $e^+e^- \to e^\mp\Sigma^\pm$, $\Sigma^0\nu$ through both the s- and t-channels, whereas the second case leads to $e^+e^- \to \mu^\mp\Sigma^\pm$, $\Sigma^0\nu$ through a purely s-channel process. As quoted in Table 2 the cross sections for the latter case are very small, and we shall not consider this in our further analysis. Figure 2 shows the cross section against the centre-of-mass energy, with the cross section for $\Sigma^0\nu$ grows to a saturation of 250 fb at around 2 TeV, while $e^\mp\Sigma^\pm$ production cross section saturates at 18 fb around 1 TeV centre-of-mass energy. For our numerical analysis we fix the centre-of-mass energy at 1 TeV, where the cross section for neutral single production is sizeable, with 187 fb. While one of the expected design centre-of-mass energies of CLIC is 1.5 TeV, we have not made a specific attempt to tune to this energy. The analyses and the conclusions are expected to be applicable at this energy as well.

The heavy fermions further decay as per Eq. (6), leading to $W\ell\nu$, $Z\nu\nu$ and $H\nu\nu$ final states in the case of Σ^0, and $W\ell\nu$, $Z\ell\ell$ and $H\ell\ell$ final states in the case of $\Sigma^\pm$ productions. With further decay of W, Z and H, this leads to the detector-level final states of $2j + \not{E}$, $2b + \not{E}$ (arising only from Σ^0 production), $2b + 2\ell$, $2j + 2\ell$, $2\ell^+ + 2\ell^-$ (arising only from $\Sigma^\pm$ production), and $2j + \ell + \not{E}$ and $2\ell + \not{E}$ (arising from both Σ^0 and $\Sigma^\pm$ productions). The lepton flavour depends on the scenarios (i) $V_e \neq 0$ or (ii) $V_\mu \neq 0$ considered, as well as on the W decay channel. Scenario (i) can lead to single flavour final states, having only electrons present, listed in Table 3 with the cross sections corresponding to these final states, along with the SM backgrounds. The cross sections quoted are the fiducial cross sections including the respective branching fractions obtained from Madgraph [48,49] with basic generation level cuts on the transverse momenta of the jets and leptons, $p_T(j) \leq 20$ GeV, $p_T(\ell) \leq 10$ GeV, and a pseudo-rapidity of $|\eta| \leq 2.5$ employed. In addition, this scenario can lead to the mixed flavour cases of $e\mu\not{E}$, $e^+e^-\mu^+\mu^-\not{E}$ with cross sections very close to those of the $e^+e^-\not{E}$, $2e^+2e^-\not{E}$ cases, respectively. Scenario (ii) will also lead to mixed flavour case of $e\mu\not{E}$ along with $\mu\, 2j\,\not{E}$ and $\mu^+\mu^-\not{E}$ final states. In the following we shall restrict ourselves to the single flavour case with only electrons and jets appearing in the final state. Coming to the backgrounds, the $2j + \not{E}$ coming from a neutral triplet has a large continuum QCD background. Similarly, the purely leptonic channel, $2e^+2e^-$, has a small cross section. We have therefore focussed on the other cases of purely leptonic and semi-leptonic final states, as well as the $b\bar{b} + \not{E}$, where the $b-$ quark pair arises from the H decay.

To analyse these selected final states, we generated 50 000 events in each case using Madgraph5 with the in-built Pythia6 [50] used for ISR, FSR, showering and hadronisation. The basic generation level cuts are those quoted above, with $p_T(j) \geq 20$ GeV, $p_T(\ell) \geq 10$ GeV, and $|\eta| \leq 2.5$ for the jets as well as leptons. These events are then passed on to Madanalysis5 [51] to analyse and optimise the final selection criteria. Fastjet [52] is used for jet reconstruction with anti-k_T algorithm and jet radius of $R = 0.4$. For the detector simulation, Delphes3 [53] with standard ILD card is used. Before

Table 3 Fiducial cross sections of signal and SM backgrounds corresponding to different final states arising from the process $e^-e^+ \to \Sigma^\pm e^\mp$ and $e^+e^- \to \Sigma^0\nu$, with $p_T(j) \geq 20$ GeV, $p_T(\ell) \geq 10$ GeV, and pseudo-rapidity $|\eta| \leq 2.5$ for jets and leptons. Centre-of-mass energy of $\sqrt{s} = 1$ TeV and $M_\Sigma = 500$ GeV are considered with the assumed mixing of $V_e = 0.05$, $V_\mu = V_\tau = 0$

Final state	Process ($e^+e^- \to \Sigma^\pm e^\mp$, $\Sigma^0\nu$)	$\sigma \times$ BR in fb	
		Signal	Background
$2j + e^- + \not{E}$	$\Sigma^+e^- \to W^+e^-\,\nu$	32.7	WWZ(0.5), WW(74.5),
	$\Sigma^0\nu \to W^+e^-\nu$		$t\tilde{t}$(1.68), ZZ(2.17), Zjj(2.77)
$2j + e^-\, e^+$	$(\Sigma^+e^- + \Sigma^-e^+) \to Ze^+e^-$	4.2	eejj(34.5)
$e^-\, e^+ + \not{E}$	$(\Sigma^+e^- + \Sigma^-e^+) \to W^\pm e^\mp\nu$, Ze^-e^+	14.8	WW(14.09), WWZ(0.036)
	$\Sigma^0\nu \to W^\pm e^\mp\nu$, $Z\nu\nu$		ZZ(0.35), $t\tilde{t}$(1.6)
$2e^- + 2e^+$	$(\Sigma^+e^- + \Sigma^-e^+) \to$ Z e^+e^-	0.3	ZZ(0.065), $eeee$(3.6)
$b\bar{b}\, e^+e^-$	$(\Sigma^+e^- + \Sigma^-e^+) \to H\, e^+e^-$	7.2	HZ(0.27), ZZ(0.78)
$b\bar{b} + \not{E}$	$\Sigma^0\nu \to H\,\nu\nu$	37.6	HZ(2.1), ZZ(8.9)
2j + $\not{E}$	$\Sigma^0\nu \to Z\,\nu\nu$	22.3	$q\bar{q}$(440.1)

Table 4 The cut-flow and signal significance for different final states arising from the single production of Σ^0 and $\Sigma^\pm$ at $\sqrt{s} = 1$ TeV and 100 fb^{-1} luminosity for processes $e^-e^+ \to \Sigma^\pm \ell^\mp$ and $e^+e^- \to \Sigma^0 \nu$, with $M_\Sigma = 500$ GeV and $V_e = 0.05,\ V_\mu = V_\tau = 0$

Final state	Selection cuts	No. of events		$\frac{S}{\sqrt{S+B}}$	$S_{\rm sys}$
	(all figures, except N are in GeV)	*Signal*	*Backgd*	$V_e = 0.05, V_\mu = V_\tau = 0$	
$2j + e^- + \not{E}$	No cut	3273	8170		
	N(j) =2, N(e^-) = 1, N(b) = 0	2187	3871		
	$p(e^-) > 100$, $p(j_1) < 300$, $p(j_2) < 200$	1681	285	37.9	17.5
$2j + e^-e^+$	No cut	420	3450		
	N(e^+) = 1, N(e^-) = 1, N(j) = 2	273	1500		
	$p(e^-)$, $p(e^+) > 140$, M(e^+e^-) > 200	270	948		
	$\eta(e^+) < 1$, $\eta(e^-) > -1$	269	110	13.8	11.1
$e^-e^+ + \not{E}$	No cut	1489	1620		
	N($e^\pm$) = 1, N(b) = 0	1103	1036		
	$\Delta R(e^+, e^-) < 4$	1014	479	26.2	14.9
$b\bar{b} + e^+e^-$	No cut	718	105		
	N(e^+) = 1, N(e^-) = 1, N(b) = 2	180	14		
	M(e^+e^-) > 140	180	0	13.4	11.1
$b\bar{b} + \not{E}$	No cut	3760	1100		
	N(e^+) = 0, N(e^-) = 0, N(b) = 2	1243	221		
	$\Delta R(b, \bar{b}) > 0.6$	1194	140	32.7	17.0

applying any selection cuts, proximity checks for the leptons are done, with leptons closer than $\Delta R_{j\ell} = 0.4$ ignored. Further selection was based on the required number of final state leptons and jets, and considering the distinguishability of the kinematic distributions. In Table 4 the cut-flow chart is presented along with the final significance that is expected at an integrated luminosity of 100 fb^{-1}. We shall briefly discuss the selection cuts of each of the final states below.

1. $2j + e^- + \not{E}$

The signal and background events after the basic generation level cuts are 3273 and 8170, respectively. After demanding that the event should contain two jets and one electron, and veto-ing the presence of b-jet, the number of events reduces to 2187 and 3871 for the signal and background, respectively. The b-jet veto is used to reduce the $t\bar{t}$ background events. This is followed by the selection of events with 100 GeV $\leq p(e^-), p(j_1) \leq 300$ GeV and $p(j_2) \leq 200$ GeV which reduces the background events to about 7%, at the same time keeping about 77% of the signal events. This leaves 285 background events against a signal of 1681. Overall, about 51% of the original signal events are retained, against about 3.5% of the background events.

Assuming only statistical uncertainty, the signal significance computed with the formula $\frac{S}{\sqrt{S+B}}$, where S is the number of signal events and B is the number of background events, is 37.9 at the luminosity of 100 fb^{-1} considered. In order to accommodate the systematic uncertainties, we have considered the following formula:

$$S_{\rm sys} = \frac{S}{\sqrt{S + B + \alpha^2\, B^2 + \beta^2\, S^2}}, \tag{7}$$

where α and β are the systematic uncertainties in the background and signal events, respectively. Systematics at leptonic colliders like ILC are expected to be well under control. Assuming a very conservative value of 5% uncertainty in both the signal and background cases, we obtain a significance of 17.5 at the integrated luminosity of 100 fb^{-1}.

2. $2j + e^-e^+$.

In this case, $p(e^-) \geq 140$ GeV and $p(e^+) \geq 140$ GeV, and a selection of invariant mass of electron–positron pairs, $M_{e^+e^-} > 200$ GeV, apart from demanding that there be one electron and one positron, and two jets are employed to reduce the background from 3450 to its 27.5%, while retaining 64.3 % of the signal events. The background is further reduced to 110 events by a selection of the pseudo-rapidity of the leptons, $\eta(e^+) < 1$ and $\eta(e^-) > -1$, leaving the signal almost unaffected. A signal significance of 13.8 and 11.1 without and with assumed systematics as above could be achieved in this case.

3. $e^-e^+ + \not{E}$

Table 5 Luminosity requirement for signal significance of 5σ for different final states of the processes $e^-e^+ \to \Sigma^\pm e^\mp$ and $e^+e^- \to \Sigma^0\nu$ at $\sqrt{s} = 1$ TeV with $M_\Sigma = 500$ GeV, for the case of $V_e = 0.05$, $V_\mu = V_\tau = 0$, along with the signal (S) and background (B) events at the specified luminosities. S_{sys} is taken as defined in Eq. (7)

Final state	for $\frac{S}{\sqrt{S+B}} = 5\sigma$			for $S_{sys} = 5\sigma$		
	$\int \mathcal{L}$ (in fb^{-1})	S	B	$\int \mathcal{L}$ (in fb^{-1})	S	B
$2j + e^- + \not{E}$	1.7	29	5	1.9	31	5
$b\bar{b} + \not{E}$	2.3	28	3	2.5	30	4
$e^-e^+ + \not{E}$	3.6	37	17	3.9	40	19
$2j + e^-e^+$	13.1	35	14	14.1	38	16
$b\bar{b} + e^+e^-$	13.9	25	0	14.8	27	0

Here, electron–positron pairs are more back to back compared to those in the signal events. Demanding lepton separation, $\Delta R(e^+, e^-) < 4$, reduces the background to 479 from 1620, while keeping 1014 signal events starting from 1489 events. This leads to a signal significance of about 26.2 without any systematics, which goes down to 14.9 with the assumed systematic uncertainties.

4. $\underline{b\bar{b} + e^- + e^+}$

A cut on the invariant mass of the lepton pair, $M_{e^+e^-} > 140$ GeV, apart from demanding two b-jets, one electron and one positron, takes away all the backgrounds, leaving 180 signal events with signal significance of 13.4 without systematics uncertainty and 11.1 with systematic uncertainty.

5. $\underline{b\bar{b} + \not{E}}$

In this case, $\Delta R(b, \bar{b}) > 0.6$ reduces the background events from 1100 to 140, while the signal is reduced from 3760 to 1194. The corresponding signal significance without systematics is 32.7, which is reduced to 17.0 with the assumed systematics.

Assuming that the kinematics of the background and signal events remains more or less the same, we can scale the luminosity to the required value for signal significance of 5σ. In Table 5 we present the projected requirement of luminosity for this case assuming only statistical uncertainty, along with the expected number of signal and background events after the selection criteria adopted as in Table 4. The $2j + e^- + \not{E}$ final state gives the best case scenario with less than 2 fb^{-1} luminosity leading to 5σ sensitivity, whereas the $2b + \not{E}$ channel can be probed at 5σ level with a little more than 2 fb^{-1} luminosity. The purely leptonic channel of $e^+e^- + \not{E}$ also requires only less than 4 fb^{-1} for this significance.

3.2 Pair production of Σ

We shall next consider the pair production of the triplet fermions. The Feynman diagrams corresponding to the production of charged fermion pairs are shown in Fig. 3. The

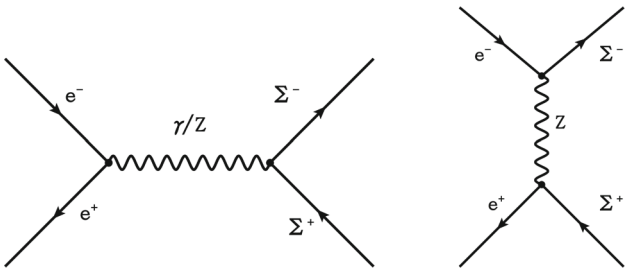

Fig. 3 Feynman diagrams contributing to the process $e^+e^- \to \Sigma^+\Sigma^-$ in isotriplet–electron mixing scenario

neutral fermion pair production also goes through the same channels, except the one with the photon exchange. Notice that the t-channel contribution to the cross section here is proportional to the fourth power of the mixing parameter V_ℓ. Thus, it is expected that the s-channel dominates. Again, the s-channel for Σ^0 pair production is proportional to the square of the $Z\Sigma^0\Sigma^0$ vertex, which is proportional to $|V_\ell|^2$. Thus, the cross section for neutral fermion pair production is very small. On the other hand, the $Z\Sigma^+\Sigma^-$ vertex is proportional to $\left(|V_\ell|^2 - 2\ \cos^2\theta_W\right) - |V_\ell|^2\ \gamma^5$, and therefore receives a sizeable contribution even in the absence of mixing. In addition, the $V_e \neq 0$ case has a t-channel contribution with the initial electron (positron) converting to Σ^- (Σ^+). However, non-zero values of $V_{\mu,\tau}$ do not lead to such a t-channel contribution. Thus the pair production process, while sensitive to V_e, is not sensitive to $V_{\mu,\tau}$. In our analyses we shall consider these two cases of (i) $V_e \neq 0$ and (ii) $V_e = 0$, with the former resulting in a slightly smaller cross section than the latter case, indicating destructive interference between the s- and the t-channel processes. We reiterate that this advantage of the FLC, where the production is sensitive to the mixing is absent at the LHC. The pair production of neutral fermions happens with very small cross section, and it is therefore difficult to probe with the expected luminosities. Therefore in the following we shall consider only the pair production of the charged fermions. The cross section against the centre-of-mass energy for the two cases considered is given in Fig. 2. The cross section peaks at about 1.2 TeV centre-of-mass energy with values of 83 fb and 119 fb

Table 6 Final state fiducial cross sections of the signal from $e^+e^- \to \Sigma^-\Sigma^+$, and the corresponding SM background processes, with the selection of $p_T(\ell) \geq 10$ GeV, pseudo-rapidity of leptons $|\eta_\ell| \leq 2.5$ and the selection of $p_T(j) \geq 20$ GeV, $|\eta_j| \leq 2.5$. Centre-of-mass energy of $\sqrt{s} = 2$ TeV, and $M_\Sigma = 500$ GeV are considered. The lepton in the final state ℓ is e or μ for the cases of $V_e = 0.05$ and $V_\mu \neq 0$, respectively

Final state	Process	$\sigma \times$ BR in fb		
	$(e^+e^- \to \Sigma^+\Sigma^-)$	Signal		Background
		$V_e = 0.05$	$V_\mu \neq 0$	
$4j + \not{E}$	$W^+W^-\nu\nu$	1.3	2.0	WWZ (1.4), $WW\nu\nu$(16.6)
$4j + \ell\ell$	$ZZ\ell^+\ell^-$	0.3	0.4	WWZ(0.15), $ZZjj$(0.7)
$4j + \ell + \not{E}$	$W^+Z\ell^-\nu$	0.6	0.8	$t\tilde{t}$(1.4), $WWjj$(0.5)
$2j + 4\ell$	$ZZ\ell^+\ell^-$	0.02	0.03	ZZZ(0.0002)
$2j + 3\ell + \not{E}$	$W^+Z\ell^-\nu$	0.04	0.05	WWZ(0.03)
$2j + 2\ell + \not{E}$	$ZZ\ell^+\ell^-$, $W^+Z\ell^-\nu$	0.4	0.5	WWZ(0.12),$t\tilde{t}$(0.44)
$2j + \ell + \not{E}$	$W^+W^-\nu\nu$, $W^+Z\ell^-\nu$	0.8	1.0	WWZ(0.27),WW(12.2), t$\tilde{t}$(1.4), ZZ(0.27)
$2\ell + \not{E}$	$W^+W^-\nu\nu$	0.1	0.2	WW(3.4), $t\bar{t}$(0.43), $\ell\ell\nu\nu$(181.7)
$2b2\bar{b} + 2\ell$	$HH\ell^+\ell^-$	1.7	2.2	HHZ(0.004)

corresponding to the cases of $V_e = 0.05$ and $V_e = 0$, respectively. At $\sqrt{s} = 2$ TeV, the cross section is reduced by a factor of 2 with 43 fb and 55.7 fb for the two cases.

While the production is not sensitive to the presence or absence of V_μ of V_τ, the decay requires one of these to be present for the second case considered above (viz. $V_e = 0$). Thus in our further analysis, we shall consider the two cases as (i) $V_e = 0.05$, $V_\mu = V_\tau = 0$ and (ii) $V_\mu \neq 0$, $V_e = V_\tau = 0$. We would like to remind our reader that the mixing entering only through the decay, as in the second case here, is not sensitive to the value of the mixing as long as the mean life of the particle is such that it decays within the detector. The dependence will cancel in the BR when only one V_ℓ is non-zero. With the decay of $\Sigma^\pm$ to $W\nu$, $Z\ell$ or $H\ell$, and the subsequent decays of W, Z and H considered, we have the purely hadronic final states of $4j + \not{E}$, semi-leptonic final states of $4j + 2\ell$, $4j + \ell + \not{E}$, $2j + 4\ell$, $2j + 3\ell + \not{E}$, $2j + 2\ell + \not{E}$, $2j + \ell + \not{E}$, $4b + 2\ell$ and the purely leptonic case of $2\ell + \not{E}$. Here $\ell = e$ for the first scenario and $\ell = \mu$ for the second one. We have included only the case of Higgs decay to a b-pair, as the other cases come with a much smaller effective cross section. Again, Z to b-pair decay is not included, and Z decaying to charged leptons is not considered, as they have very small cross section. In Table 6 the cross sections of these final states arising from the signal for the two cases considered are given, along with the corresponding SM background cross sections. The cross sections are obtained from the MC simulation with Madgraph5 with Pythia6 used for hadronisation and showering. We have included the generation level basic cuts on the transverse momenta of jets and leptons of $p_T(j) > 20$ GeV and $p_T(\ell) > 10$ GeV, and considered jets and leptons with a pseudo-rapidity of $|\eta| < 2.5$. The final states with $2j + 4\ell$ and $2j + 3\ell + \not{E}$ have very small cross sections and, therefore, very large luminosities are required to probe these channels. The purely leptonic final state of $2\ell + \not{E}$ comes with large SM background of about three orders larger than the signal. Thus, in our further analysis we do not consider these three cases.

As in the case of single triplet production, the events generated are then passed on to Madanalysis5, using Fastjet for jet reconstruction with anti-k_T algorithm and jet radius of $R = 0.4$. Detector simulation was carried out with the help of Delphes3 with standard ILD card. Before applying any selection cuts, proximity checks for leptons were done with leptons closer than $\Delta R_{j\ell} = 0.4$ to the jets ignored. Further selection was based on the required number of final state leptons and jets, and considering the distinguishability of the kinematic distributions. In the $4j$ events, we considered two different situations with (i) setting the number of jets exactly equal to four, and (ii) demanding every event has three jets or more. The second case lead to marginal improvement in the significance, and about double the signal events in each case. In Table 7 the cut-flow chart is presented along with the final significance that is expected at an integrated luminosity of 300 fb^{-1}. We shall briefly discuss the cuts used to optimise the selection below.

1. $4j + \not{E}$

With $p(j_1) > 100$ GeV, the two cases of $N(j) = 4$ and $N(j) \geq 3$ give significances of 3.4 and 5.4, respectively, for the scenario with $V_e = 0.05$ when only statistical errors are assumed. This is reduced to 1.5 and 1.7, respectively, with the assumed systematics of 5% on both the signal and background event determination. The scenario with $V_e = 0$ has the corresponding significances of 5 (2) and 7.5 (2.4) considering statistical (statistical plus systematic) uncertainty.

Table 7 Number of surviving events, and signal significance for different final states arising from the pair production of $\Sigma^{\pm}\Sigma^{\mp}$ at $300\,fb^{-1}$ luminosity at $\sqrt{s} = 2$ TeV, and $M_{\Sigma} = 500$ GeV. $S_{\rm sys}$ corresponds to the signal significance with assumed systematics according to Eq. (7)

Final state	Selection cuts	$V_e = 0.05$			$V_\mu \neq 0$				
	(All dimensional quantities are in GeV)	Signal S	Backd B	$\frac{S}{\sqrt{S+B}}$	$S_{\rm sys}$	Signal B	Backd B	$\frac{S}{\sqrt{S+B}}$	$S_{\rm sys}$
$4j + \not{E}$	$N(j) = 4,\ p(j_1) > 100$	147	1679	3.4	1.5	243	2164	5	2
	$N(j) \geq 3,\ p(j_1) > 100$	353	3914	5.4	1.7	503	3914	7.5	2.4
$4j + \ell^{\pm} + \not{E}$	$N(\ell^{\pm}) = 1,\ N(j) = 4,\ N(b) = 0$ $p(\ell^{\pm}) > 100,\ \not{E} > 100$	50	12	6.3	6	73	13	7.8	7.3
	$N(\ell^{\pm}) = 1,\ N(j) \geq 3,\ N(b) = 0$ $p(\ell^{\pm}) > 100,\ \not{E} > 100$	106	33	8.9	8.1	154	39	11.1	9.6
$4j + \ell^{+}\ell^{-}$	$N(\ell^{\pm}) = 1,\ N(j) = 4,$ $p(\ell^{\pm}) > 100,\ \Delta R(\ell^{+}, \ell^{-}) \geq 2$	29	0	5.3	5.2	74	0	8.6	7.9
	$N(\ell^{\pm}) = 1,\ N(j) \geq 3,$ $p(\ell^{\pm}) > 100,\ \Delta R(\ell^{+}, \ell^{-}) \geq 2$	56	0	7.4	7	140	0	11.8	10.1
$2j + \ell^{+}\ell^{-} + \not{E}$	$N(\ell^{+}) = 1,\ N(\ell^{-}) = 1,\ N(j) = 2,$ $N(b) = 0,\ p(\ell^{-}) > 100$	47	12	6.1	5.8	54	15	6.5	6.1
$2j + \ell^{\pm} + \not{E}$	$N(\ell^{\pm}) = 1,\ N(j) = 2,\ N(b) = 0,$ $\lvert\eta(\ell)\rvert < 1,\ p(\ell) < 900$ $p(j_1) < 600,\ p(j_2) < 300$	87	365	4.0	3.0	121	10	10.5	9.3
$4b + \ell^{+}\ell^{-}$	$N(\ell^{+}) = 1,\ N(\ell^{-}) = 1,$ $N(b) = 4,\ p(e^{\pm}) > 60$	24	0	4.9	4.7	34	0	5.8	5.5
	$N(\ell^{+}) = 1,\ N(\ell^{-}) = 1,$ $N(b) \geq 3,\ p(e^{\pm}) > 60$	114	0	10.6	9.4	163	0	12.7	10.8

Notice that this channel is purely hadronic, and it does not leave any trace of the type of mixing involved.

2. $4j + \ell^{\pm} + \not{E}$

Here ℓ is an electron or a muon depending on the case of $V_e \neq 0$ or $V_\mu \neq 0$. Unlike the case of $4j + \not{E}$, here the missing energy has a different topology in signal compared to that of the background (refer to Table 6 for the list of major backgrounds). Cuts of $p(\ell) > 100$ GeV and $\not{E} > 100$ GeV are used apart from demanding one lepton and $N(j) = 4$ or $N(j) \geq 3$, along with demanding $N(b) = 0$ to reduce the $t\bar{t}$ background. The significance for the case of electron are 6.3 (6) and 8.9 (8.1) without (with) systematics assumed, for the two cases of jet counting of (i) $N(j) = 4$ and (ii) $N(j) \geq 3$, respectively. In the case of a muon, these are 7.9 (7.3) and 11.1 (9.6), respectively. Notice that the systematics have a less pronounced effect here, as the events are small in number. We assume the charge of the lepton is identified, with the two cases giving similar results.

3. $4j + \ell^{+}\ell^{-}$

In this final state, the oppositely charged dileptons originate at the production in signal, whereas they come from the decay of Z bosons in the case of the backgrounds. Therefore, the leptons are expected to be more energetic in the case of signal events. We employ a cut of $p(\ell^{\pm}) > 100$ GeV in both the cases of $N(j) = 4$ and $N(j) \geq 3$. In addition, we have assumed that the two leptons are separated with $\Delta R \geq 2$, as they are expected to be well separated in the case of signal events, whereas in the case of background events they will be more collimated as they originate from the Z boson in flight. With these selection cuts, the background is practically eliminated. The significance for the four and three jet counting is 5.3 and 7.5 for electrons, and 8.6 and 11.8, respectively, for the case of muons. As the events are not very large, the systematics do not have much effect here.

4. $2j + 2\ell + \not{E}$

Coming to the $2j + \ell + \not{E}$ events, $p(\ell^{-}) > 100$ GeV is employed after demanding exactly two jets and two oppositely charged same-flavour leptons, leading to a significance of 6.1 and 6.5 for the case of electron and muon, respectively. Here again, the systematics have only a small role to play.

5. $2j + \ell^{\pm} + \not{E}$

The major background here is the WW production with the semi-leptonic decay of the pair. The lepton coming from the W is expected to be very energetic, unlike the case of the signal. A cut on the energy of the lepton, $p(\ell) < 900$ GeV is employed, along with a cut on the pseudo-rapidity of lepton $|\eta(\ell)| < 1$, reduced the background considerably. Further cuts on the momenta of jets $p(j_1) < 600$ GeV and $p(j_2) <$

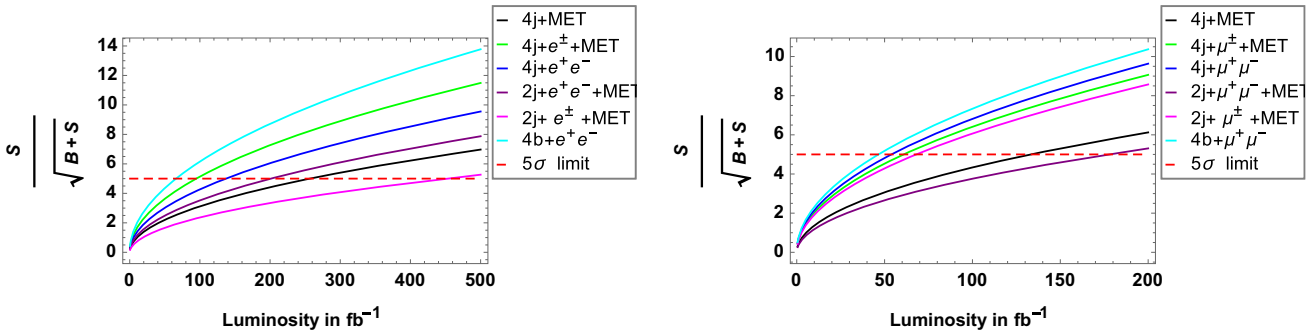

Fig. 4 Signal significance of different final states from pair production of $\Sigma^{\pm}$ against integrated luminosity at $\sqrt{s} = 2$ TeV. Mass of triplet fermion, $M_{\Sigma} = 500$ GeV and mixing parameters of $V_e = 0.05$ (left) and $V_{\mu} \neq 0$ (right) are considered with other mixings set to zero

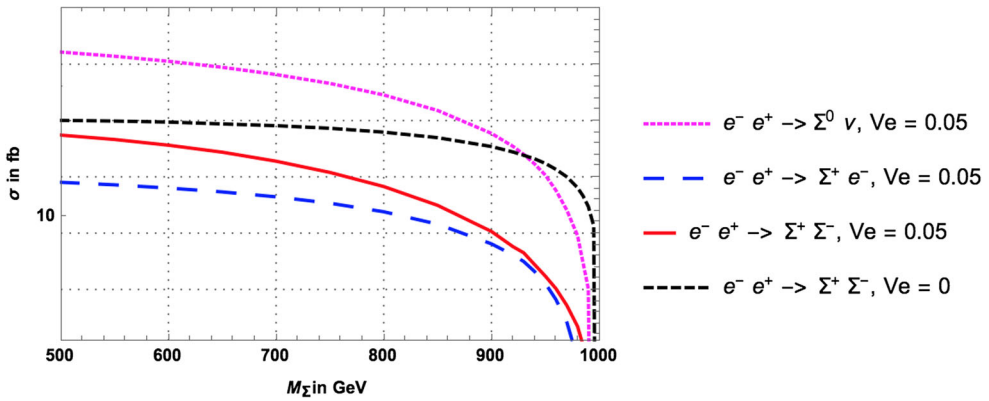

Fig. 5 Dependence of the cross section on the mass of fermions for pair and single production. Single production is considered at $\sqrt{s} = 1$ TeV, whereas $\sqrt{s} = 2$ TeV is considered for a pair production process. Mixing is considered as indicated, with $V_{\mu} = V_{\tau} = 0$ in all cases

300 GeV are considered to reach an expected significance of 4 (3) for electron without (with) systematics considered. The case of muons presents a much better scenario with an expected significance of 10.6 (9.3).

6. $4b + 2\ell$

The background for the $4b$ events is quite suppressed. We have considered identifying two oppositely charged leptons, and the cases of $N(b) = 4$ and $N(b) \geq 3$, along with demanding $p(e^{\pm}) > 60$ GeV. The numbers of events surviving in the case of electron mixing are 24 and 114, respectively, with vanishing backgrounds in both cases. In the case of muon mixing, the significance is improved with the surviving number of events of 34 and 163, respectively.

Summarising, $4j + 2\ell$ and $4b + 2\ell$ provide the best case scenarios, where practically no background events are present. Both of these cases could also distinguish the mixing scenarios from the flavour of the leptons produced. The single lepton events with missing energy accompanied by either four jets or two jets also provide very promising scenarios. Here the four jet case can distinguish the two mixing scenarios with the flavour identification, whereas the two jet case has the leptons arising also from the W decay, and therefore, it will give a mixed signal.

All the final states in both the cases with two different mixing scenarios are used to indicate the projected luminosity required for 5σ significance in Fig. 4. A luminosity of less than 300 fb^{-1} is sufficient to probe all the channels with electron in the final state (except $2j + e^{\pm} + \not{E}$) at 5σ level. On the other hand $4j + \not{E}$ and $2j + \mu^{+}\mu^{-} + \not{E}$ require about 130 and 180 fb^{-1} luminosity, whereas all other channels with μ in the final state can be explored at 5σ level with less than 100 fb^{-1} luminosity.

3.3 Dependence on the mass of Σ

So far in the analysis we had fixed the mass of the heavy fermion to $M_{\Sigma} = 500$ GeV. This section will explore the mass dependence for a specific choice of mixing at a given centre-of-mass energy. The cross sections for single and pair productions considered at the centre-of-mass energies of 1 and 2 TeV, respectively, are presented in Fig. 5 against M_{Σ}. The near threshold behaviour of the pair production with $V_e = 0$ is distinctly different from the case with $V_e \neq 0$. This may be attributed to the fact that, while the former case

Table 8 The mass reach at 2 TeV with integrated luminosity of 300 fb^{-1} from selected channels of pair production of charged fermions, giving 3σ sensitivity. The corresponding production cross sections $\sigma(\Sigma^+\Sigma^-)$, and the number of signal (S) and background (B) events after employing the selection criteria are also given. Only a single flavour with $\ell = e,\ \mu$ is considered for the cases of $V_e = 0.05$ and $V_\mu \neq 0$, respectively

Final state	$V_e = 0.05$				$V_\mu \neq 0$			
	S	B	$\sigma(\Sigma^+\Sigma^-)$ in fb	M_Σ in GeV	S	B	$\sigma(\Sigma^+\Sigma^-)$ in fb	M_Σ in GeV
$4b + 2\ell$	9	0	3.4	945	9	0	3.0	997
$4j + 2\ell$	9	0	6.9	910	9.2	0.17	3.6	995
$4j + \ell^\pm + \not{E}$	16	33.3	9.1	885	23.7	38.5	8.5	990
$2j + \ell + \not{E}$	62	365	30.7	660	15	9.7	6.9	992

Table 9 The mass reach at 1 TeV with integrated luminosity of 100 fb^{-1} from selected channels of single production of charged and neutral fermions, giving 3σ sensitivity. The corresponding production cross sections $\sigma(\Sigma^\pm e^\mp)$, $\sigma(\Sigma^0\nu)$ and the number of signal (S) and background (B) events after employing the selection criteria are also given

Final state	S	B	$\sigma(\Sigma^+e^-)$ in fb	M_Σ in GeV	Final state	S	B	$\sigma(\Sigma^0\nu)$ in fb	M_Σ in GeV
$2j + e^-e^+$	37	110	2.5	956	$b\bar{b} + \not{E}$	40.4	140.3	6.3	982
$b\bar{b} + e^-e^+$	9	0	0.92	978					

is a purely s-channel process, the latter has a contribution from the t-channel as well, facilitated by the presence of $Z\Sigma e$ coupling. The single production cases are presented only for $V_e \neq 0$ case, as the Σe production is not possible with $V_e = 0$, while $\Sigma\nu$ production is very small in the case of $V_\mu \neq 0$. The mass dependence seems to follow the same pattern in the two cases of neutral as well as the charged fermion single production considered here. We shall now demonstrate that with 300 fb^{-1} integrated luminosity, the reach of ILC is close to $M_\Sigma = 1$ TeV. Let us consider the case of $4b+2\ell$ final state in the $\Sigma^+\Sigma^-$ pair production with a cross section of 43 fb at $\sqrt{s} = 2$ TeV with an assumed mixing of $V_e = 0.05$ and a mass of $M_\Sigma = 500$ GeV. The selection criteria considered in this study leave 114 signal events with an integrated luminosity of 300 fb^{-1}. This corresponds to an effective cross section times branching ratio of 0.38 fb. The selection cuts have eliminated the background, and thus the number of signal events required for 3σ signal significance is about 9, corresponding to a cross section times branching ratio of $\frac{9}{300} = 0.03$. Assuming that the selection cuts behave the same way, the production cross section required to get this significance is $\frac{43}{0.38} \times 0.03 = 3.39$ fb. At $\sqrt{s} = 2$ TeV, keeping $V_e = 0.05$, this cross section corresponds to a mass of $M_\Sigma = 950$ GeV. A similar study of the $4j + 2\ell$ and $4j + \ell + \not{E}$ final states shows that about 3σ significance is reached with a pair production cross section of 6.9 and 9.1 fb, respectively. These correspond to mass reaches of about 910 and 885 GeV, respectively. Considering the μ channels with $V_\mu \neq 0$ (as explained earlier, the results do not depend on the value of V_μ); the situation gets somewhat better with the addition of $2j + \ell + \not{E}$ also enabling one to probe the model with M_Σ very close to the kinematic limit of 1000 GeV. Table 8 summarises the mass reach at a 2 TeV ILC with an integrated luminosity of 300 fb^{-1}.

The mass reach estimated to be achieved through the single production process at $\sqrt{s} = 1$ TeV with an integrated luminosity of 100 fb^{-1} for selected final states (arising through single production channel) is given in Table 9. With the two selected channels of $2j + e^+e^-$ and $2b + e^+e^-$ arising from $\Sigma^\pm e^\mp$ production, and the final state $2b + \not{E}$ arising from $\Sigma^0\nu$ could probe the model with M_Σ close to 1 TeV, assuming $V_e = 0.05$.

4 Dependence on the mixing

The limiting cross sections required for 3σ significance listed in Tables 8 and 9 are exploited to extract the two-parameter contours in the $V_e - M_\Sigma$ plane. As mentioned earlier, in the case when only V_μ is non-zero, the process including the decay rates does not depend on the value of the mixing. On the other hand, both the single and pair productions are sensitive to the value of V_e. Table 8 lists the limiting cross sections for 3σ significance in the case of different final states arising from the pair production. It may be noted that the pair production process has a large contribution from the gauge coupling, and the presence of non-zero mixing results in destructive interference, thus reducing the cross section from its value when $V_e = 0$. In Fig. 6 regions of the production cross section, $\sigma > 30.7$ fb are indicated in blue colour. The M_Σ–V_e two-parameter limits obtainable from the final state $2j + e + \not{E}$ are indicated by the boundary of this blue region. Similarly, the 3σ limits of M_Σ–V_e obtained from $4j + e + \not{E}$ final state are indicated by the boundary between the green

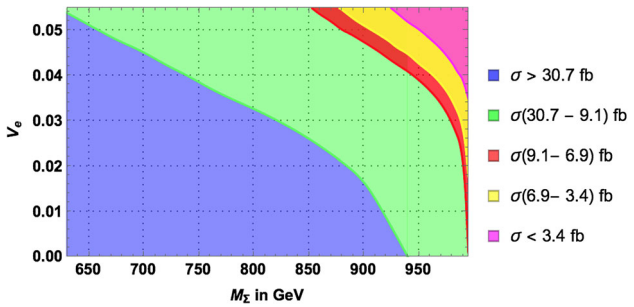

Fig. 6 Regions of M_Σ–V_e plane with different ranges of cross section values for pair production at 2 TeV centre-of-mass energy as indicated. The ranges of cross sections are the 3σ limiting values given in Table 8

and red regions, and those from $4j + e^+e^-$ and $4b + e^+e^-$ are given by the boundaries of red and yellow regions, and yellow and pink regions, respectively. The $2j + e + \not{E}$ channel is capable of probing the entire range of presently allowed values of V_e for varying value of M_Σ. On the other hand, the other channels, $4j + e + \not{E}$, $4j + e^+e^-$, and $4b + e^+e^-$ will not be able to probe below $M_\Sigma \sim 850,\ 875,\ 925$ GeV.

Coming to the single production of Σ, the cross section vanishes in the absence of V_ℓ. In Fig. 7 regions of different cross section values corresponding to the limiting cases of 3σ limits obtainable from different final states are indicated in the M_Σ–V_e plane. The case of Σe production is shown in the left figure, with the boundary between blue and green regions showing the two-parameter limits obtainable from the $2j + e^+e^-$ channel, whereas the boundary between green and orange regions indicating the limits from the $2b + e^+e^-$ final state. In the figure on the right the two-parameter limits from $2b + \not{E}$ resulting from $\Sigma^0\nu$ is indicated by the boundary of the green and grey regions. The channels of $2b + e^+e^-$ and $2b + \not{E}$ can probe V_e to 0.04 to 0.01, depending on the value of M_Σ, whereas the final state, $2j + e^+e^-$, is slightly less sensitive.

5 Summary and conclusions

The Type-III seesaw mechanism proposed to generate a tiny neutrino mass provides an example of physics beyond the SM scenario with heavy leptons. We study the direct production of heavy leptons at a high energy e^+e^- collider through possible final states arising from their subsequent decays. Present direct searches at the LHC limit the masses of such heavy fermions in the range of 500 GeV or above. While the LHC is capable of discovering the presence of heavy leptons in the TeV mass range, it is hard to probe the details of the couplings involving mixing with the SM leptons. On the other hand, high energy e^+e^- colliders like the ILC or CLIC with electrons in the initial state are suitable for this purpose, where the production process itself is sensitive to the mixing. While the simple Type-III seesaw models required small Yukawa couplings, and consequently small mixing, we imagine a broader scenario with additional mechanism to generate a small neutrino mass despite the presence of large mixing, and we explore the collider consequence that may follow. Thus the conclusions drawn in this work are applicable to any scenario where there exists a heavy lepton which mixes with the SM leptons, as long as any additional spectrum arising in such scenario does not affect the decay branching ratio of the heavy leptons, possibly because such resonances are heavier, and thus beyond the reach of TeV energy colliders.

Investigating the single and pair production of the neutral as well as charged leptons at e^+e^- collider at centre-of-mass energies of 1 TeV and 2 TeV, respectively, this work performed detailed detector-level analyses to identify interesting final states, and the achievable significance for selected parameter choices.

Single charged (neutral) triplet fermions are produced in association with a charged (neutral) SM leptons or a neutrino. Consequently these processes are absent in the case when Σ does not have any mixing with the SM leptons. In order to avoid FCNC constraints, in our study we assume

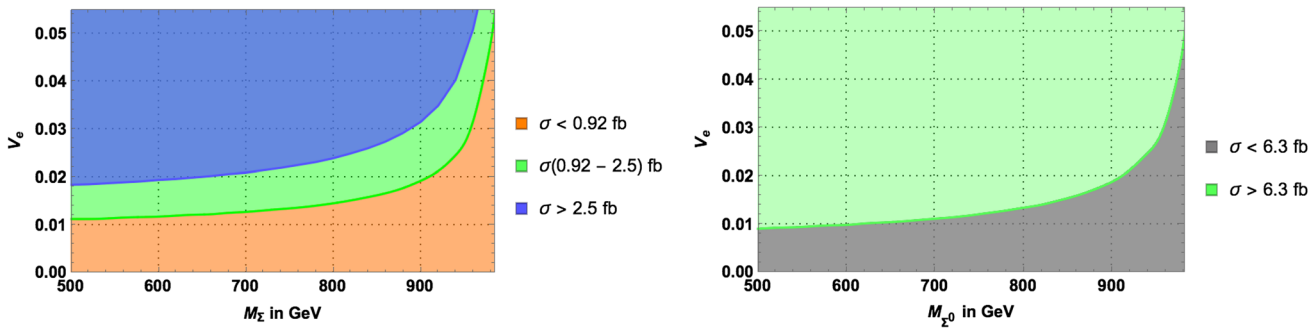

Fig. 7 Regions of the M_Σ–V_e plane with different ranges of cross section values for single production at 1 TeV centre-of-mass energy as indicated. The figure on the left corresponds to $\Sigma^\pm e^\mp$ production, and that on the right corresponds to $\Sigma^0\nu$ production. The ranges of the cross sections are the 3σ limiting values given in Table 9

that the triplets mix with either electron (V_e) or muon (V_μ), and not both. The case of mixing with the tau lepton in not considered in this work as we focus on final states involving only electrons, muons and jets. Study of $\Sigma^\pm\ell^\mp$ and $\Sigma^0\nu$ production shows that the cross section in the case of $V_\mu \neq 0$ is negligibly small. Focussing on the triplet–electron mixing scenario, we first studied the most optimistic case of $V_e = 0.05$ and $M_\Sigma = 500$ GeV, fixing these parameters at their present experimental limits. Performing a full detector simulation, considering all the SM backgrounds for various detector-level final states arising from Σe and $\Sigma\nu$, we find that $2j + e^- + \not{E}$, $2b + \not{E}$ and $e^+e^- + \not{E}$ could be probed at 5σ significance (assuming only statistical uncertainty) with 2 to 4 fb^{-1} luminosity. Among the other final states, the $2j + e^+e^-$ and $2b + e^+e^-$ channels require about 14 to 15 fb^{-1} luminosity for 5σ significance. Extrapolating this result to higher values of M_Σ, we found that a 1 TeV e^+e^- collider with 100 fb^{-1} luminosity could probe the mass very close to the kinematic limit of about 950 to 980 GeV, assuming $V_e = 0.05$.

Coming to the pair production, the cross section for Σ^0 pair production turns out to be negligibly small. On the other hand, the $\Sigma^+\Sigma^-$ production process is present even in the absence of mixing, as the gauge coupling dictates the strength of the $Z\Sigma^+\Sigma^-$ coupling, leading to pair production through the s-channel process. The presence of mixing provides only a very negligible addition to this in the s-channel. The production is practically insensitive to the triplet mixing with a muon or tau lepton. In the scenario with $V_e \neq 0$ an additional t-channel opens the avenue to discriminate this case with the case of $V_e = 0$. In the latter case, we have considered $V_\mu \neq 0$ so as to facilitate the decay of the triplet to the SM leptons. However, the dependence on V_μ, when present alone, is cancelled in the BR. Thus we carried out our analysis in the two scenarios of (i) $V_e = 0,\ V_\mu \neq 0$ and (ii) $V_e \neq 0,\ V_\mu = 0$. The analysis was performed with all possible detector-level final states arising from the pair production and subsequent decays. Cross sections of multi-lepton channels with more than two leptons in the final state, and the purely leptonic channel of $2\ell + \not{E}$ are very small, and therefore were not considered in this analysis. Among the other channels, the best case scenario is given by the $4b + 2\ell$ channels coming from the $H\ell$ decay of Σ, requiring about 50 fb^{-1} luminosity for 5σ significance in both the scenarios considered. In all cases, the first scenario with triplet–muon mixing provides better sensitivity, mostly because of the larger cross section available. The final states of $4j + \mu^+\mu^-$, $4j + \mu + \not{E}$ and $2j + \mu + \not{E}$ can be probed at 5σ level with luminosities of 50, 60 and 70 fb^{-1}, respectively, whereas their counterparts in the $V_e \neq 0$ case replacing μ with an electron require luminosities of 140, 100 and 460 fb^{-1}, respectively. The difference between the two scenarios can be attributed to the distinctions in muon and electron identification and efficiencies, as well as to the slightly different kinematic distributions in the two cases. The $2j + \ell\ell + \not{E}$ final state, on the other hand, does not seem to favour any scenario, requiring moderate luminosities of about 200 fb^{-1} in the case of $V_e \neq 0$, and 175 fb^{-1} in the case of $V_\mu \neq 0$. This may be due, again, to the fact that the cross sections are almost the same in the two cases. The purely hadronic case of $4j + \not{E}$ has a much better background compared to the other channels (except the $4b + 2\ell$ case), but it suffers from efficiencies involved in the jet formation and identification, thus requiring slightly larger luminosities of 260 and 130 in the cases of $V_e \neq 0$ and $V_\mu \neq 0$, respectively. Coming to the reach of M_Σ through the pair production, the two channels, $4b + e^+e^-$ and $4j + e^+e^-$ could probe beyond 900 GeV with 300 fb^{-1} luminosity, whereas all the channels with muonic final states could probe very close to the kinematic reach, going above 990 GeV.

Probing the sensitivity to the mixing parameter, V_e, we obtained two-parameter limits achievable by different final states from single and pair productions. The single production channels are capable of probing low mass regions for small mixing values, going up to 0.01 for the triplet–electron mixing parameter in the case of masses close to 500 GeV with $2b + e^+e^-$ and $2b + \not{E}$ arising from Σe and $\Sigma^0\nu$, respectively. The pair production, on the other hand can probe smaller values of mixings for larger $M - \Sigma$ values, where the best suitable final state is $2j + e + \not{E}$.

The study has clearly demonstrated the potential of a high energy e^+e^- collider to probe the presence of heavy leptons, and the details of their couplings with the SM particles, thus supporting the case for such leptonic collider even with successful running of the LHC. Considering the nature of the process, in the presence of t-channel production in some of the mixing scenarios, we anticipate that beam polarisation could be utilised to enhance the sensitivity. A study of the effect of beam polarisation, as well as a detailed analysis to understand the reach of the coupling, is deferred to a future publication.

Acknowledgements This work is partly supported by the BRNS, DAE, Govt. of India project (2010/37P/49/BRNS/1446), and the SERB, DST of India project (EMR/2015/000333). The authors are thankful to Dr. Sumit K. Garg for useful discussions and involvement in the initial stage of the work.

Open Access This article is distributed under the terms of the Creative Commons Attribution 4.0 International License (http://creativecommons.org/licenses/by/4.0/), which permits unrestricted use, distribution, and reproduction in any medium, provided you give appropriate credit to the original author(s) and the source, provide a link to the Creative Commons license, and indicate if changes were made.
Funded by SCOAP[3].

6 Appendix

A1: The Lagrangian

The Lagrangian of the Type-III seesaw model in the mass basis is given by

$$\mathcal{L} = \mathcal{L}_{Kin}+\mathcal{L}_{CC}+\mathcal{L}^{\ell}_{NC}+\mathcal{L}^{\nu}_{NC}+\mathcal{L}^{\ell}_{H}+\mathcal{L}^{\nu}_{H}+\mathcal{L}^{\ell}_{\eta}+\mathcal{L}^{\nu}_{\eta}+\mathcal{L}_{\phi^-}, \tag{8}$$

where $\mathcal{L}_{Kin}$ is the kinetic part and

$$\mathcal{L}_{CC} = \frac{g}{\sqrt{2}}\left(\bar{\ell}\ \overline{\Psi}\right)\gamma^{\mu}\ W^{-}_{\mu}\left(P_L\ g^{CC}_{L} + P_R\ g^{CC}_{R}\sqrt{2}\right)\begin{pmatrix}\nu\\ \Sigma\end{pmatrix} + h.c \tag{9}$$

$$\mathcal{L}^{\ell}_{NC} = \frac{g}{\cos\theta_W}\left(\bar{\ell}\ \overline{\Psi}\right)\gamma^{\mu}Z_{\mu}\left(P_L\ g^{NC}_{L} + P_R\ g^{NC}_{R}\right)\begin{pmatrix}\ell\\ \Psi\end{pmatrix} \tag{10}$$

$$\mathcal{L}^{\nu}_{NC} = \frac{g}{2\cos\theta_W}\left(\bar{\nu}\ \overline{\Sigma}^{0c}\right)\gamma^{\mu}Z_{\mu}\left(P_L\ g^{NC}_{\nu}\right)\begin{pmatrix}\nu_L\\ \Sigma^{0c}\end{pmatrix}, \tag{11}$$

$$\mathcal{L}^{\ell}_{H} = -\left(\bar{\ell}\ \overline{\Psi}\right)H\left(P_L\ g^{H\ell}_{L} + P_R\ g^{H\ell}_{R}\right)\begin{pmatrix}\ell\\ \Psi\end{pmatrix}, \tag{12}$$

$$\mathcal{L}^{\nu}_{H} = -\left(\bar{\nu}\ \overline{\Sigma}^{0}\right)\frac{H}{\sqrt{2}}\left(P_L\ g^{H\nu}_{L} + P_R\ g^{H\nu}_{R}\right)\begin{pmatrix}\nu\\ \Sigma^{0}\end{pmatrix}, \tag{13}$$

$$\mathcal{L}^{\ell}_{\eta} = -\left(\bar{\ell}\ \Psi\right)i\eta\left(P_L\ g^{\eta\ell}_{L} + P_R\ g^{\eta\ell}_{R}\right)\begin{pmatrix}\ell\\ \Psi\end{pmatrix}, \tag{14}$$

$$\mathcal{L}^{\nu}_{\eta} = -\left(\bar{\nu}\ \overline{\Sigma}^{0}\right)\frac{i\eta}{\sqrt{2}}\left(P_L\ g^{\eta\nu}_{L} + P_R\ g^{\eta\nu}_{R}\right)\begin{pmatrix}\nu\\ \Sigma^{0}\end{pmatrix}, \tag{15}$$

$$\mathcal{L}_{\phi^-} = -\left(\bar{\ell}\ \overline{\Psi}\right)\phi^{-}\left(P_L\ g^{\phi^-}_{L} + P_R\ g^{\phi^-}_{R}\right)\begin{pmatrix}\nu\\ \Sigma^{0}\end{pmatrix} + h.c., \tag{16}$$

where the left and right projection operates are denoted by $P_{L,R} = \frac{1}{2}(1 \mp \gamma_5)$. The couplings, g_i are explicitly given below in terms of the other parameters of the original Lagrangian. Here, the fields and the couplings, g_i are given in block matrix form, with

$$\begin{pmatrix}\ell\\ \Psi\end{pmatrix} \equiv \begin{pmatrix}e\\ \mu\\ \tau\\ \Psi\end{pmatrix} \text{ and } \begin{pmatrix}\nu\\ \Sigma\end{pmatrix} \equiv \begin{pmatrix}\nu_e\\ \nu_\mu\\ \nu_\tau\\ \Sigma^0\end{pmatrix},$$

$$g^{CC}_{L} = \begin{pmatrix}\left(1+\frac{\epsilon}{2}\right)U_{\rm PMNS} & -\frac{\upsilon}{\sqrt{2}M_\Sigma}Y^{\dagger}_{\Sigma}\\ 0 & \sqrt{2}\left(1-\frac{\epsilon'}{2}\right)\end{pmatrix}, \tag{17}$$

$$g^{CC}_{R} = \begin{pmatrix}0 & -\frac{m_\ell \upsilon}{M^2_\Sigma}Y^{\dagger}_{\Sigma}\\ -\frac{\upsilon}{\sqrt{2}M_\Sigma}Y^{*}_{\Sigma}U^{*}_{\rm PMNS} & 1-\frac{\epsilon'^{\star}}{2}\end{pmatrix}, \tag{18}$$

$$g^{NC}_{L} = \begin{pmatrix}\frac{1}{2}-\cos^2\theta_W-\epsilon & \frac{\upsilon}{2M_\Sigma}Y^{\dagger}_{\Sigma}\\ \frac{\upsilon}{2M_\Sigma}Y_{\Sigma} & \epsilon'-\cos^2\theta_W\end{pmatrix}, \tag{19}$$

$$g^{NC}_{R} = \begin{pmatrix}1-\cos^2\theta_W & \frac{m_\ell \upsilon}{M^2_\Sigma}Y^{\dagger}_{\Sigma}\\ \frac{m_\ell \upsilon}{M^2_\Sigma}Y_{\Sigma} & -\cos^2\theta_W\end{pmatrix}, \tag{20}$$

$$g^{NC}_{\nu} = \begin{pmatrix}1-U^{\dagger}_{\rm PMNS}\,\epsilon\,U_{\rm PMNS} & \frac{\upsilon}{\sqrt{2}\,M_\Sigma}U^{\dagger}_{\rm PMNS}Y^{\dagger}_{\Sigma}\\ \frac{\upsilon}{\sqrt{2}M_\Sigma}Y_{\Sigma}U_{\rm PMNS} & \epsilon'\end{pmatrix}, \tag{21}$$

$$g^{H\ell}_{L} = \begin{pmatrix}\frac{m_\ell}{\upsilon}(1-3\epsilon) & \frac{m_\ell Y^{\dagger}_{\Sigma}}{M_\Sigma}\\ Y_{\Sigma}\left(1-\epsilon+\frac{m^2_\ell}{M^2_\Sigma}\right) & \frac{\upsilon}{M_\Sigma}Y_{\Sigma}Y^{\dagger}_{\Sigma}\end{pmatrix}, \tag{22}$$

$$g^{H\ell}_{R} = (g^{H\ell}_{L})^{\dagger}, \tag{23}$$

$$g^{H\nu}_{L} = \begin{pmatrix}-\frac{\sqrt{2}\,m^d_\nu}{\upsilon} & \frac{m_\nu}{M_\Sigma}U^{T}_{\rm PMNS}Y^{\dagger}_{\Sigma}\\ Y_{\Sigma}(1-\frac{\epsilon}{2}-\frac{\epsilon'}{2})U_{\rm PMNS} & \frac{\upsilon}{\sqrt{2}M_\Sigma}Y_{\Sigma}Y^{\dagger}_{\Sigma}\end{pmatrix}, \tag{24}$$

$$g^{H\nu}_{R} = (g^{H\nu}_{L})^{\dagger}, \tag{25}$$

$$g^{\eta\ell}_{L} = \begin{pmatrix}-\frac{m_\ell}{\upsilon}(1+\epsilon) & -\frac{m_\ell}{M_\Sigma}Y^{\dagger}_{\Sigma}\\ Y_{\Sigma}(1-\epsilon-\frac{m^2_\ell}{M^2_\Sigma}) & \frac{\upsilon}{M_\Sigma}Y^{\dagger}_{\Sigma}Y_{\Sigma}\end{pmatrix}, \tag{26}$$

$$g^{\eta\ell}_{R} = -\left(g^{\eta\ell}_{L}\right)^{\dagger}, \tag{27}$$

$$g^{\eta\nu}_{R} = -\left(g^{\eta\nu}_{L}\right)^{\dagger}, \tag{28}$$

$$g^{\eta\nu}_{L} = g^{H\nu}_{L}, \tag{29}$$

$$g^{\phi^-}_{L} = \begin{pmatrix}\sqrt{2}\frac{m_\ell}{\upsilon}(1-\frac{\epsilon}{2})U_{\rm PMNS} & \frac{m_\ell}{M_\Sigma}Y^{\dagger}_{\Sigma}\\ \frac{\sqrt{2}m^2_\ell}{M^2_\Sigma}Y_{\Sigma}U_{\rm PMNS} & 0\end{pmatrix}, \tag{30}$$

$$g^{\phi^-}_{R} = \begin{pmatrix}-\frac{\sqrt{2}m^{d*}_\nu}{\upsilon}U_{\rm PMNS} & Y^{\dagger}_{\Sigma}(1-\epsilon-\frac{\epsilon'^{\star}}{2}-\frac{2m^{\star}_\nu}{M_\Sigma})\\ -\sqrt{2}Y^{*}_{\Sigma}(1-\frac{\epsilon^{\star}}{2})U^{\star}_{\rm PMNS} & 2\left(-\frac{M_\Sigma}{\upsilon}\epsilon'+\epsilon'\frac{M_\Sigma}{\upsilon}\right)\end{pmatrix}. \tag{31}$$

Here, $\upsilon \equiv \sqrt{2}\langle\phi^0\rangle$ is the vev of the doublet scalar field, $\epsilon = \frac{\upsilon^2}{M^2_\Sigma}Y^{\dagger}_{\Sigma}Y_{\Sigma}$, $\epsilon' = \frac{\upsilon^2}{2M^2_\Sigma}\sum_\ell Y^2_{\Sigma\ell}$ and $U_{\rm PMNS}$ is the lepton mixing matrix. The Yukawa coupling matrix $Y_\Sigma = \left(Y_{\Sigma e}\ Y_{\Sigma\mu}\ Y_{\Sigma\tau}\right)$, where $Y_{\Sigma\ell}$ are the Yukawa couplings appearing in Eq. (1). The mixing of Σ with the SM leptons is denoted by $V_\ell = \frac{\upsilon}{\sqrt{2}M_\Sigma}Y_{\Sigma\ell}$, where $\ell = e, \mu, \tau$.

A2: Cross sections for single and pair productions of fermions

The expressions of the invariant amplitudes for the pair and single production of charged and neutral fermions are given below, with the general expression of the cross section given by

$$\frac{d\sigma}{dt} = (4\pi\alpha)^2\frac{|M|^2}{16\pi s^2}.$$

1. Process $e^+e^- \to \Sigma^-\Sigma^+$

The invariant amplitude for the pair production of charged fermions can be written as

$$|M|^2 = \frac{|M_{s\gamma}|^2}{s^2}$$

$$+\frac{1}{\cos^4\theta_W \sin^4\theta_W}\left(\frac{|M_t|^2}{(t-m_Z^2)^2}+\frac{|M_{sz}|^2}{(s-m_Z^2)^2}\right)$$
$$+\frac{1}{\cos^4\theta_W \sin^4\theta_W}\left(\frac{M_{int}^{szt}}{(s-m_Z^2)(t-m_Z^2)}\right)$$
$$+\frac{1}{\cos^2\theta_W \sin^2\theta_W}\left(\frac{M_{int}^{\gamma z}}{s(s-m_Z^2)}+\frac{M_{int}^{\gamma t}}{s(t-m_Z^2)}\right), \quad (32)$$

where

$$|M_t|^2 = \left(g_{L14}^{NC}\right)^4\left(64\left((s+t)^2+m_\Sigma^2(m_\Sigma^2-2s-2t)\right)\right.$$
$$\left.+\frac{s^2}{m_Z^2}\left(4s+t^2+\frac{m_\Sigma^4}{m_Z^2}-2t\frac{m_\Sigma^2}{m_Z^2}\right)(1-\beta^2)^2\right),$$
$$|M_{sz}|^2 = 64\ g_{L44}^{NC}\ g_{R44}^{NC}\left(\left(g_{R11}^{NC}\right)^2+\left(g_{L11}^{NC}\right)^2\right)$$
$$\times(m_\Sigma^4 - s\,m_\Sigma^2 - 2tm_\Sigma^2 + t^2)$$
$$+64\left((g_{R11}^{NC}\ g_{R44}^{NC})^2+(g_{L11}^{NC}\ g_{L44}^{NC})^2\right)$$
$$\times(m_\Sigma^4 - s\,m_\Sigma^2 - 2t\,m_\Sigma^2 + (s+t)^2),$$
$$|M_{s\gamma}|^2 = 8s(s+2t)+16\,(t-m_\Sigma^2)^2,$$
$$M_{int}^{szt} = \frac{g_{L11}^{NC}\ (g_{L14}^{NC})^2}{m_Z^2}\left(32\ g_{R44}^{NC}\ m_\Sigma^2\left((t-m_\Sigma^2)^2-2sm_Z^2\right)\right.$$
$$\left.+\ g_{L44}^{NC}\left(32s\left((2s+2t-1)-(s+t)^2\right)-\frac{s^4}{m_Z^2}(1-\beta^2)^2\right)\right),$$
$$M_{int}^{\gamma z} = 32\left(g_{L11}^{NC}\ g_{L44}^{NC}+g_{R11}^{NC}\ g_{R44}^{NC}\right)$$
$$\times\left(s(s-m_\Sigma^2+2t)+(m_\Sigma^2-t)^2\right)$$
$$+32\left(g_{L11}^{NC}\ g_{R44}^{NC}+g_{L44}^{NC}\ g_{R11}^{NC}\right)\left(sm_\Sigma{}^2+(m_\Sigma^2-t)^2\right),$$
$$M_{int}^{\gamma t} = (g_{L14}^{NC})^2\left(32m_\Sigma^2\ (s+2t-m_\Sigma^2)-32(s+t)^2\right.$$
$$\left.-\frac{s^3}{m_Z^2}(1-\beta^2)^2-\frac{16m_\Sigma^2}{m_Z^2}\ (m_\Sigma^2-t)^2\right).$$

Here, M_t is the invariant amplitude for the t-channel process, M_{sz} and $M_{s\gamma}$ are invariant amplitudes for s-channel processes with Z boson and photon propagators, respectively (see Fig. 3). M_{int}^{szt} gives the interference of the t-channel with the s-channel with the Z boson propagator. $M_{int}^{\gamma z}$ and $M_{int}^{\gamma t}$ give the interference of the s-channel having a photon propagator with the s-channel having a Z boson, and the t-channel processes, respectively. The factors g_{ij} are the corresponding elements of the coupling matrix given in Eq. (17)–(31), and the boost variable β in the above expressions can be written as $\beta = \sqrt{1-\frac{4M_\Sigma^2}{s}}$.

2. Process $e^+(p_1)e^-(p_2) \to \Sigma^0(p_3)\nu_\ell(p_4)$

The invariant amplitude for the single production of neutral fermions can be written (with $t = (p_1 - p_3)^2$) as

$$|M|^2 = \frac{1}{\cos^4\theta_W \sin^4\theta_W}\left(\frac{|M_t|^2}{(t-m_Z^2)^2}\right.$$
$$\left.+\frac{|M_s|^2}{(s-m_Z^2)^2}+\frac{M_{int}^{ts}}{(t-m_Z^2)(s-m_Z^2)}\right) \quad (33)$$

where

$$|M_t|^2 = \left(\left(g_{R11}^{NC}\ g_{R14}^{NC}\right)^2+\left(g_{L11}^{NC}\ g_{L14}^{NC}\right)^2\right)$$
$$\times\left(\beta^2\ (64s^4-32ts)+\beta^4\ (16t^2-32ts)\right)$$
$$+64\ s^2\beta^2\left(g_{L14}^{NC}\ (g_{R11}^{NC})^2\ g_{R14}^{NC}+g_{L14}^{NC}\ (g_{L11}^{NC})^2\ g_{R14}^{NC}\right),$$
$$|M_s|^2 = \left(\left(g_{R11}^{NC}\ g_{R14}^{NC}\right)^2+\left(g_{L11}^{NC}\ g_{L14}^{NC}\right)^2\right)$$
$$\times\left(\beta^2\ (64\ s^2-32t\ s)+\beta^4\ (16\ t^2-32\ t\ s)\right)$$
$$+\left(g_{L14}^{NC}\ (g_{R11}^{NC})^2\ g_{R14}^{NC}+(g_{L14}^{NC}\ g_{R11}^{NC})^2\right)$$
$$\times\left(32\ ts\beta^2-\beta^4(16t^2-32ts)\right)$$
$$M_{int}^{ts} = \left(\left(g_{R11}^{NC}\ g_{R14}^{NC}\right)^2+\left(g_{L11}^{NC}\ g_{L14}^{NC}\right)^2\right)$$
$$\times\left((64\ t\ s-128s^2)\beta^2+(64\ t\ s-32\ t^2)\beta^4\right).$$

Here again, M_t, M_s are invariant amplitudes for the t-channel, s-channel with a Z boson propagator and M_{int}^{ts} is the interference term involving the t- and s-channel with the Z boson propagator shown in Fig. 1. β in the above expressions can be written as $\beta = \frac{s-M_\Sigma^2}{s+M_\Sigma^2}$.

3. Process $e^+(p_1)e^-(p_2) \to \Sigma^-(p_3)e^+(p_4)$

The invariant amplitude for the single production of charged fermions can be written (with $t = (p_1 - p_3)^2$) as

$$|M|^2 = \frac{|M_\gamma|^2}{s^2}+\frac{1}{4\sin^4\theta_W}\ \frac{|M_t|^2}{(t-m_W^2)^2}$$
$$+\frac{1}{4\cos^4\theta_W \sin^4\theta_W}\ \frac{|M_s|^2}{(s-m_Z^2)^2}$$
$$+\frac{1}{2\sin^2\theta_W}\ \frac{M_{int}^{gtW}}{s(t-m_W^2)}$$
$$+\frac{1}{4\cos^2\theta_W \sin^4\theta_W}\ \frac{M_{int}^{ztW}}{(t-m_W^2)(s-m_Z^2)}$$
$$+\frac{1}{2\cos^2\theta_W \sin^2\theta_W}\ \frac{M_{int}^{gz}}{s(s-m_Z^2)}, \quad (34)$$

where

$$|M_t|^2 = \left(\left(g_{R1\ell}^{CC}\ g_{R14}^{CC}\right)^2+\left(g_{L1\ell}^{CC}\ g_{L14}^{CC}\right)^2\right)$$
$$\times\left(\beta^2\ (64\ s^2-32\ t\ s)+\beta^4\ (16\ t^2-32\ t\ s)\right)$$
$$+64\ s^2\beta^2\ \left(\left(g_{R1\ell}^{CC}\ g_{L14}^{CC}\right)^2+\left(g_{L1\ell}^{CC}\ g_{R14}^{CC}\right)^2\right),$$

$$
\begin{aligned}
|M_s|^2 &= 16\, t\, \beta^4\, (g_{\nu 14}^{NC})^2 (t-2s) \left((g_{R11}^{NC})^2 + (g_{L11}^{NC})^2 \right) \\
&\quad +32 s\, \beta^2\, (g_{\nu 14}^{NC})^2 (2s-t) \left((g_{L11}^{NC})^2 + 32 ts (g_{R11}^{NC})^2 \right), \\
|M_\gamma|^2 &= 4\beta^2 (s^2 + t\beta^2 (t-2s)), \\
M_{int}^{ztW} &= 32\, \beta^2 (2s - \beta^2\, t)(t-2s) \left(g_{L1\ell}^{CC}\, g_{L14}^{CC}\, g_{L11}^{NC}\, g_{\nu 14}^{NC} \right), \\
M_{int}^{gtW} &= 8\, \beta^2 (t-2s)(2s - t\beta^2) \left(g_{R1\ell}^{CC}\ g_{R14}^{CC} + g_{L1\ell}^{CC}\ g_{L14}^{CC} \right), \\
M_{int}^{gz} &= \beta^4\, (g_{\nu 14}^{NC})\, (8t^2 - 16\, t\, s) \left(g_{R11}^{NC} + g_{L11}^{NC} \right) \\
&\quad +\beta^2\, g_{\nu 14}^{NC} \left(64\, t\, s\, (g_{R11}^{NC} - g_{L11}^{NC}) + 32\, s^2\, g_{L11}^{NC} \right).
\end{aligned}
$$

Here, M_t, M_s, M_γ are the invariant amplitudes with the propagator of the W boson (t-channel), Z boson and photon, respectively. M_{int}^{ztW} is the invariant amplitude of interference terms of the s-channel with Z boson propagator and the t-channel with W boson propagator. M_{int}^{gtW} is the invariant amplitude of the interference term with the s-channel containing the photon propagator and the t-channel containing the W boson propagator. M_{int}^{gz} is the invariant amplitude of the interference term having the s-channel with the Z boson and the photon propagator (see Fig. 1). β in the above expressions is given by $\beta = \frac{s - M_\Sigma^2}{s + M_\Sigma^2}$.

References

1. P. Minkowski, Phys. Lett. B **67**, 421 (1977)
2. M. Gell-Mann, P. Ramond, R. Slansky (1980)
3. T. Yanagida, in *Proceedings of the Workshop on the Baryon Number of the Universe and Unified Theories*, Tsukuba (1979)
4. J. Schechter, J.W.F. Valle, Phys. Rev. D **22**, 2227 (1980)
5. T. Yanagida, in *Proceedings of Workshop on Unified theory and Baryon Number in the Universe*, ed. by O. Sawada, A. Sugamoto (KEK, 1979)
6. M. Gell-Mann, P. Ramond, R. Slansky, in *Supergravity*, ed. by P. van Nieuwenhuizen, D. Freedman (North- Holland, Amsterdam, CERN, 1980)
7. Y. Chikashige, R.N. Mohapatra, R.D. Peccei, Phys. Lett. **98B**, 265 (1981)
8. P.A.R. Ade et al., Planck Collaboration. Astron. Astrophys. **571**, A16 (2014). arXiv:1303.5076 [astro-ph.CO]
9. R.N. Mohapatra, G. Senjanovic, Phys. Rev. D **163**, 23 (1981)
10. G. Lazarides, Q. Shafi, C. Wetterich, Nucl. Phys. B **181**, 287 (1981)
11. C. Wetterich, Nucl. Phys. B **187**, 343 (1981)
12. J. Schechter, J.W.F. Valle, Phys. Rev. D **25**, 774 (1982)
13. B. Brahmachari, R.N. Mohapatra, Phys. Rev. D **58**, 015001 (1998)
14. R.N. Mohapatra, Nucl. Phys. Proc. Suppl. **138**, 257 (2005)
15. S. Antusch, S.F. King, Phys. Lett. B **597**(2), 199 (2004)
16. R. Foot, H. Lew, X.G. He, G.C. Joshi, Z. Phys. C **44**, 441 (1989)
17. T. Barklow, J. Brau, K. Fujii, J. Gao, J. List, N. Walker, K. Yokoya, arXiv:1506.07830 [hep-ex]
18. T. Behnke et al., arXiv:1306.6327 [physics.acc-ph]
19. H. Baer et al., arXiv:1306.6352 [hep-ph]
20. C. Adolphsen et al., arXiv:1306.6353 [physics.acc-ph], arXiv:1306.6328 [physics.acc-ph]
21. C. Bartels, A. Hartin, C. Helebrant, D. Kafer, J. List, Nucl. Instrum. Methods A **623**, 570 (2010)
22. B. Vormwald, JINST **9**, C08012 (2014). arXiv:1406.3636 [physics.ins-det]
23. C. Helebrant, D. Kafer, J. List, arXiv:0809.4485 [physics.ins-det]
24. G. Moortgat-Pick, T. Abe, G. Alexander, B. Ananthanarayan, A.A. Babich, V. Bharadwaj, D. Barber, A. Bartl et al., Phys. Rep. **460**, 131 (2008)
25. J. Brau et al. [ILC Collaboration], arXiv:0712.1950 [physics.acc-ph]
26. G. Aarons et al. [ILC Collaboration], arXiv:0709.1893 [hep-ph]
27. A. Sailer, EPJ Web Conf. **70**, 00085 (2014)
28. H. Abramowicz et al., arXiv:1307.5288 [hep-ex]
29. M. Aicheler et al., CERN-2012-007
30. P. Lebrun et al., CERN-2012-005
31. B. Bajc, M. Nemevsek, G. Senjanovic, Phys. Rev. D **76**, 055011 (2007). arXiv:hep-ph/0703080
32. R. Franceschini, T. Hambye, A. Strumia, Phys. Rev. D **78**, 033002 (2008). arXiv:0805.1613 [hep-ph]
33. F. del Aguila, J.A. Aguilar-Saavedra, Nucl. Phys. B **813**, 22 (2009). arXiv:0808.2468 [hep-ph]
34. T. Li, X.G. He, Phys. Rev. D **80**, 093003 (2009). arXiv:0907.4193 [hep-ph]
35. P. Bandyopadhyay, S. Choi, E.J. Chun, K. Min, Phys. Rev. D **85**, 073013 (2012). arXiv:1112.3080 [hep-ph]
36. O.J.P. Eboli, J. Gonzalez-Fraile, M.C. Gonzalez-Garcia, JHEP **1112**, 009 (2011). arXiv:1108.0661 [hep-ph]
37. F. von der Pahlen, G. Palacio, D. Restrepo, O. Zapata, Phys. Rev. D **94**, 033005 (2016). arXiv:1605.01129 [hep-ph]
38. R. Ruiz, JHEP **1512**, 165 (2015). https://doi.org/10.1007/JHEP12(2015)165. arXiv:1509.05416 [hep-ph]
39. CMS Collaboration [CMS Collaboration], CMS-PAS-EXO-16-002
40. The ATLAS collaboration, Search for type III Seesaw model heavy fermions in events with four charged Leptons using 5.8 fb^{-1} of $\sqrt{s} = 8$ TeV data with the ATLAS Detector. ATLAS Collaboration ATLAS-CONF-2013-019 (2013). http://atlas.web.cern.ch/Atlas/GROUPS/PHYSICS/CONFNOTES/ATLAS-CONF-2013-019/. Accessed 17 Jan 2018
41. G. Aad et al. [ATLAS Collaboration], Phys. Rev. D **92**(3), 032001 (2015). arXiv:1506.01839 [hep-ex]
42. H. Liang, X.G. He, W.G. Ma, S.M. Wang, R.Y. Zhang, JHEP **1009**, 023 (2010). arXiv:1006.5534 [hep-ph]
43. C.-X. Yue, H.-L. Feng, W. Ma, Chin. Phys. Lett. **27**, 011202 (2010)
44. C. Biggio, F. Bonnet, Eur. Phys. J. C **72**, 1899 (2012). arXiv:1107.3463 [hep-ph]
45. A. Abada, C. Biggio, F. Bonnet, M.B. Gavela, T. Hambye, Phys. Rev. D **78**, 033007 (2008). arXiv:0803.0481 [hep-ph]
46. A. Abada, C. Biggio, F. Bonnet, M.B. Gavela, T. Hambye, JHEP **0712**, 061 (2007). arXiv:0707.4058 [hep-ph]
47. F. del Aguila, J. de Blas, M. Perez-Victoria, Phys. Rev. D **78**, 013010 (2008). arXiv:0803.4008 [hep-ph]
48. J. Alwall, M. Herquet, F. Maltoni, O. Mattelaer, T. Stelzer, JHEP **1106**, 128 (2011). arXiv:1106.0522 [hep-ph]
49. J. Alwall et al., JHEP **1407**, 079 (2014)
50. T. Sjostrand, S. Mrenna, P.Z. Skands, JHEP **0605**, 026 (2006)
51. E. Conte, B. Fuks, G. Serret, Comput. Phys. Commun. **184**, 222 (2013). arXiv:1206.1599 [hep-ph]
52. M. Cacciari, G.P. Salam, G. Soyez, Eur. Phys. J. C **72**, 1896 (2012). https://doi.org/10.1140/epjc/s10052-012-1896-2. arXiv:1111.6097 [hep-ph]
53. J. de Favereau et al., DELPHES 3 Collaboration, JHEP **1402**, 057 (2014). arXiv:1307.6346 [hep-ex]